Attenuation of Neurovirulence, Biodistribution, and Shedding of a Poliovirus:Rhinovirus Chimera after Intrathalamic Inoculation in *Macaca fascicularis*

Elena Y. Dobrikova,[a] Christian Goetz,[a] Robert W. Walters,[a] Sarah K. Lawson,[a] James O. Peggins,[b] Karen Muszynski,[c] Sheryl Ruppel,[d] Karyol Poole,[d] Steven L. Giardina,[d] Eric M. Vela,[e] James E. Estep,[e] and Matthias Gromeier[a]

Division of Neurosurgery, Department of Surgery, Duke University Medical Center, Durham, North Carolina, USA[a]; Toxicology and Pharmacology Branch, National Cancer Institute, Frederick, Maryland, USA[b]; Biological Research Branch, National Cancer Institute, Frederick, Maryland, USA[c]; Biopharmaceutical Development Program, SAIC-Frederick, Inc., NCI-Frederick, Frederick, Maryland, USA[d]; and Battelle, Columbus, Ohio, USA[e]

A dependence of poliovirus on an unorthodox translation initiation mode can be targeted selectively to drive viral protein synthesis and cytotoxicity in malignant cells. Transformed cells are naturally susceptible to poliovirus, due to widespread ectopic upregulation of the poliovirus receptor, Necl-5, in ectodermal/neuroectodermal cancers. Viral tumor cell killing and the host immunologic response it engenders produce potent, lasting antineoplastic effects in animal tumor models. Clinical application of this principle depends on unequivocal demonstration of safety in primate models for paralytic poliomyelitis. We conducted extensive dose-range-finding, toxicity, biodistribution, shedding, and neutralizing antibody studies of the prototype oncolytic poliovirus recombinant, PVS-RIPO, after intrathalamic inoculation in *Macaca fascicularis*. These studies suggest that intracerebral PVS-RIPO inoculation does not lead to viral propagation in the central nervous system (CNS), does not cause histopathological CNS lesions or neurological symptoms that can be attributed to the virus, is not associated with extraneural virus dissemination or replication and does not induce shedding of virus with stool. Intrathalamic PVS-RIPO inoculation induced neutralizing antibody responses against poliovirus serotype 1 in all animals studied.

Several years ago, we proposed consideration of recombinant, nonpathogenic poliovirus (PV) for the treatment of glioblastoma (GBM) (17). This proposal is based on widespread ectopic expression of the PV receptor, nectin-like molecule-5 (Necl-5), in such cancers (26). Necl-5, an onco-fetal cell adhesion molecule of the nectin family, is broadly associated with ectodermal/neuroectodermal cancers (reviewed in reference 42). Necl-5 expression is abundant in GBM cells, "stem cell-like" GBM cells, and tumor-associated vasculature (6) and is implicated in GBM cell dispersion and invasion (39, 40). Due to Necl-5 expression, GBM cells are naturally susceptible to infection with and rapid destruction by PV (17). Direct cytocidal effects of PV elicit host immunogenic responses directed against tumors *in vivo* (43).

Any clinical application of engineered PVs must include a rigorous demonstration of safety in established nonhuman primate models for paralytic poliomyelitis. Such safety studies are modeled after standard neurovirulence assays for the live-attenuated (Sabin) PV vaccines (41). The three Sabin vaccine serotypes (PV1-S, PV2-S, and PV3-S), some stemming from serial passage in diverse simian tissue culture systems, exhibit substantially reduced primate neurovirulence (36). While the genetic base for attenuation is different for each Sabin strain (29), they have key sequence variables in common.

PV plus-strand RNA genomes are not equipped with a 7-methyl-guanidine cap (31) and thus are unable to recruit ribosomal subunits via the cap-binding eukaryotic initiation factor (eIF) 4E. Instead, PV RNAs rely on an internal ribosomal entry site (IRES) within their 5′ untranslated region (UTR) to recruit 40S ribosomal subunits internally, in a 5′ cap-, eIF4E-independent manner (21, 34). This occurs by direct binding of the central scaffold of the translation initiation apparatus and "ribosome adaptor" eIF4G to the IRES (8). Intriguingly, the three Sabin serotypes feature point mutations within a defined region of IRES stem-loop domain (SLD) V (45) that may impede eIF4G binding and, hence, virulence in normal neuronal cells (8, 33). The Sabin SLD V mutations are critical attenuation determinants, since reversion restores neurovirulence (12, 23). Accordingly, in cases of Sabin vaccine-associated poliomyelitis, reversion of the IRES attenuating mutation to the wild-type (wt) sequence is invariably detected in the culprit virus isolated from affected patients.

Non-neurovirulence of the PV variant studied here does not rely on IRES point mutations but on a heterologous IRES derived from human rhinovirus type 2 (HRV2) (15). Insertion of the HRV2 IRES into wt PV1, yielding PV1-RIPO, reduced neuronal competence below the levels of PV1-S, evident as poor replication potential in neuroblastoid cell lines, e.g., Sk-N-Mc (15) or HEK-293 (5, 14). Accordingly, PV1-RIPO lacked neurovirulence in the World Health Organization (WHO) standard neurovirulence test after intraspinal inoculation in *Macaca fascicularis* (16). Remarkably, HRV2 IRES substitution alone achieves attenuation levels similar to PV1-S (the PV1-S consensus sequence features 57 potentially attenuating mutations, 21 of which result in coding changes [32]). Studies with PV1:HRV2 mix-and-match IRES recombinants suggest a mechanistic base for attenuation similar to the Sabin attenuating SLD V mutations, since viral competence in neuronal cells covaries with IRES portions implicated in eIF4G binding (5, 16).

TABLE 1 Sampling intervals for the IND-directed toxicology study of PVS-RIPO

Procedure	Study day															
	−7	0	3	7	10	12	14	15	18	21	25	28	35	43	49	56
Virus injection		x														
Body wt	x	x	x	x	x		x			x		x	x	x	x	x
Temp	x	x	x	x	x	x	x	x	x	x	x	x	x	x	x	x
Blood collection	x	x	x		x		x			x		x		x		x
Clinical chemistry/hematology	x	x	x		x		x			x		x		x		x
Serum (α-PV ab)		x	x		x							x				x
Serum (viremia)		x	x		x		x					x				x
Saliva		x					x					x		x		x
Urine		x					x					x		x		x
Stool			x		x	x	x	x	x	x	x	x	x	x	x	x
Ophthalmic exam	x						x					x		x		x
Complete physical			x		x											x
Necropsy			x		x											x

To derive a maximally attenuated PV, we inserted the HRV2 IRES into PV1-S, yielding PVS-RIPO (10). We report here on dose-range-finding, toxicology, biodistribution, shedding, and neutralizing antibody studies of PVS-RIPO after intrathalamic challenge in *M. fascicularis*.

MATERIALS AND METHODS

Viruses and 50% tissue culture infective dose (TCID$_{50}$) assay. PV1-S was derived from a cDNA clone (GenBank accession no. V01150) (32), kindly provided by A. Nomoto (University of Tokyo, Tokyo, Japan), using standard procedures described elsewhere (15). The PV1-S consensus sequence was used as the backbone for constructing PVS-RIPO (10). PV1-S was propagated in Vero cells, purified by two high-speed centrifuge spins, and resuspended in Dulbecco modified Eagle medium (DMEM). PVS-RIPO is PV1-S containing a heterologous IRES of HRV2, which was inserted as described previously (15). PVS-RIPO used in the dose-range-finding study was from toxicology lot L0603006 and the good-manufacturing-practice (GMP) clinical lot L0904010 was used in the definitive Investigational New Drug application (IND)-directed studies. Both lots were produced at the Biopharmaceutical Development Program, SAIC-Frederick, Inc. (10). Virus titers were quantified by a tissue culture infectious dose assay (i.e., TCID$_{50}$) on Hep-2C indicator cells (obtained from SAIC-Frederick, Inc.) according to the WHO standard procedure (46, 47). Viruses were diluted in phosphate-buffered saline (PBS) for laboratory assays and in GMP-manufactured vehicle (50 mM sodium phosphate, 0.9% sodium chloride, 0.2% human serum albumin) for all animal experiments.

Growth assays in primate primary kidney cultures. Primary *M. fascicularis* kidney epithelial (cynomolgus macaque kidney [CMK]) cells (Diagnostic Hybrids) and primary human renal epithelial cells (CC-2556; Cambrex BioScience) were obtained at their first passage (direct subcultivation of cells from processed tissues). CMK and human renal cells were grown in a One Renal Epithelial Cell BulletKit (Cambrex BioScience) according to the manufacturer's instructions. All assays were performed with cells at their second *ex vivo* passage. The cells were seeded at a density of 2,500 cells/cm² in six-well plates and incubated at 37°C until achieving ~90% confluence. Prior to the growth curve experiments, the cultures were rinsed with DMEM (Invitrogen). The experimental setup was a standard one-step growth curve (13). Briefly, cells in a control well were treated with trypsin and counted using a hemocytometer to determine the amount of virus needed to achieve a multiplicity of infection (MOI) of 10. PVS-RIPO or PV1-S at the desired concentration (as determined by a TCID$_{50}$ assay) was suspended in DMEM, and 500 μl of virus suspension was added to the wells at an MOI of 10. The culture dishes were gently rocked for 30 min at room temperature and rinsed three times with

DMEM to remove unattached virus. All cultures (except the 0-h time points) were transferred to incubators at 37°C. The cultures were removed from the incubators at 4, 8, 12, 24, and 48 h after incubation. The cultures were freeze-thawed three times, and the resulting lysate was analyzed by TCID$_{50}$ assay.

Intrathalamic inoculation of PVS-RIPO in *M. fascicularis*. Animal studies were performed at Battelle, Columbus, OH. All procedures were reviewed and approved by the Institutional Animal Care and Use Committee. Macaques (male or female; 1.3 to 2.5 kg [dose-range-finding study] and 2.2 to 3.4 kg [definitive IND-directed study]) were randomly assigned to study groups. Animals were screened for antibodies against all three PV serotypes, simian virus 40, herpes B virus, tuberculosis, simian T-cell leukemia virus, simian retrovirus, and simian immunodeficiency virus. Intrathalamic dosing of PVS-RIPO followed standard procedures. Briefly, anesthetized animals were placed on an inoculation table with a sighting device for proper alignment of the head along the horizontal and vertical axes. A template outlining the drill sites was placed on the head along the horizontal and vertical axis. An incision was created near the junction of the sagittal and coronal sutures and an appropriate drill was used to drill a hole through the cranium. Test article in a volume of 250 μl was inserted to the hub, and the inoculum was injected.

Clinical tests, hematological analyses, clinical chemistry, and sample collection. Identical testing procedures were used in the dose-range-finding and IND-directed studies. The study days and sampling intervals mentioned (Table 1) apply to animals enrolled in the IND-directed study only. Baseline temperatures were measured by sensor chips implanted in the shoulder and leg regions on study day −7. Temperatures were recorded 3 ± 1 h after dosing on study day 0 and at the intervals indicated thereafter (Table 1). Baseline body weights were recorded on study day −7 and as indicated thereafter (Table 1). Daily clinical exams included observations of the general condition, skin, fur, eyes, ears, nose, oral cavity, thorax, abdomen, external genitalia, limbs, feet, and neurological status and evaluation of respiration. Quantitative food consumption was recorded daily starting on study day −7. On study days 3, 10, and 56, the animals underwent complete physicals and neurological exams, consisting of, but not limited to, observations for hunched posture, lethargy, incoordination, weakness, anisochoria, state of confound, fasciculations, lacrimation, miosis, mydriasis, nystagmus, salivation, tremors, convulsions, responsiveness, and prostration (Table 1). Blood was collected from a femoral vein or artery hematology and clinical chemistry assessment on study day −7 (baseline) and as indicated thereafter (Table 1). Hematological parameters, including white or red blood cell counts, hemoglobin, hematocrit, mean corpuscular volume/hemoglobin/hemoglobin concentration, red cell distribution width, platelet count, mean platelet volume, and differential leukocyte counts were analyzed on an Advia 120 hemato-

TABLE 2 DRF toxicology study of PVS-RIPO

Animal	Dose ($TCID_{50}$), volume, route	Euthanasia (day)	Biodistribution studies conducted[a]
A29114	0, 250 μl, intrathalamic	3	Complete biodistribution, stool shedding
A29098	0, 250 μl, intrathalamic	21	Complete biodistribution, stool shedding
A29135	$1 \times 10e7$, 250 μl, intrathalamic	3	None
A29136	$1 \times 10e7$, 250 μl, intrathalamic	21	Complete biodistribution, stool shedding
A29091	$1 \times 10e9$, 250 μl, intrathalamic	3	None
A28814	$1 \times 10e9$, 250 μl, intrathalamic	21	Complete biodistribution, stool shedding
A29159	$5 \times 10e9$, 250 μl, intrathalamic	3	Complete biodistribution, stool shedding
A28838	$5 \times 10e9$, 250 μl, intrathalamic	21	None
A29092	$5 \times 10e9$, 250 μl, intrathalamic	21	Complete biodistribution, stool shedding

[a] Studies included biodistribution assays using the tissue panel shown in Table 4 ("complete biodistribution") and $TCID_{50}$/plaque assays for stool samples ("stool shedding") obtained at study days 2, 4, 7, 14, and 21. The results of either assay were identical to the test results in the IND-directed study and are not discussed in detail.

logical analyzer (Siemens). Clinical chemistry, including glucose, blood urea nitrogen (BUN), creatinine, BUN/creatinine ratio, sodium, potassium, chloride, calcium, phosphorous, total bilirubin, total protein, albumin, globulin, albumin/globulin ratio, alanine/aspartate amino transferases, alkaline phosphatase, gamma glutamyl transferase, sorbitol dehydrogenase, was analyzed on an Advia 1200 serum chemistry analyzer (Siemens). Serum, saliva, urine, and stool specimens were collected as indicated in Table 1.

Necropsy and histopathology. Animals were euthanized as indicated in Tables 2 and 3. All euthanized primates underwent necropsy and complete postmortem examination. Two sets of samples of the tissues listed in Table 4 (see the table for the complete biodistribution analyses) were collected. One set was frozen for later analyses of virus biodistribution, and one set was fixed in cold, buffered neutral 10% formalin. Histopathology was performed on tissue samples fixed in cold, buffered neutral 10% formalin and processed for paraffin embedding. The embedded tissue blocks were sectioned at a thickness of 5 μm and processed for hematoxylin-eosin or gallocyanin histological stains. Macaque brains were dissected and freed of all surrounding tissues, fixed, and processed into sagittal slices of approximately 5 to 8 mm width using a nonhuman primate brain matrix. Microscopic evaluations focused on the area of the inoculum and the surroundings of the needle track. The needle track was identified by locating the characteristic lesion on the brain surface and the associated tissue reaction surrounding the injection channel. Horizontal sections were prepared through each cerebral hemisphere at the level of the thalamus, such that three blocks per hemisphere per animal included the entire thalamus from bottom (ventral) to top (dorsal/superior). Each whole-brain slice, including the rostral-most and most posterior regions of the hemisphere, enabled a complete evaluation of the thalamus. The entire hemisphere from front to back in each section was evaluated. Five

TABLE 3 IND-directed toxicology study of PVS-RIPO

Animal	Group: dose ($TCID_{50}$), vol, route	Euthanasia (day)	Study result[a]
A08404	1: 0, 250 μl, intrathalamic	3	Complete biodistribution
A10102	1: 0, 250 μl, intrathalamic	3	None
A09134	1: 0, 250 μl, intrathalamic	10	Complete biodistribution
A07639	1: 0, 250 μl, intrathalamic	10	None
A06682	1: 0, 250 μl, intrathalamic	56	Select biodistribution, neutralizing antibodies
A06953	1: 0, 250 μl, intrathalamic	56	Neutralizing antibodies
A09731	2: $5 \times 10e7$, 250 μl, intrathalamic	3	None
A10091	2: $5 \times 10e7$, 250 μl, intrathalamic	3	None
A10171	2: $5 \times 10e7$, 250 μl, intrathalamic	3	None
A10174	2: $5 \times 10e7$, 250 μl, intrathalamic	3	None
A09131	2: $5 \times 10e7$, 250 μl, intrathalamic	10	None
A09160	2: $5 \times 10e7$, 250 μl, intrathalamic	10	None
A09723	2: $5 \times 10e7$, 250 μl, intrathalamic	10	None
A09732	2: $5 \times 10e7$, 250 μl, intrathalamic	10	None
A08411	2: $5 \times 10e7$, 250 μl, intrathalamic	56	None
A09252	2: $5 \times 10e7$, 250 μl, intrathalamic	56	None
A10093	2: $5 \times 10e7$, 250 μl, intrathalamic	56	None
A10095	2: $5 \times 10e7$, 250 μl, intrathalamic	56	None
A08132	3: $1 \times 10e9$, 250 μl, intrathalamic	3	Complete biodistribution
A08760	3: $1 \times 10e9$, 250 μl, intrathalamic	3	Complete biodistribution
A09763	3: $1 \times 10e9$, 250 μl, intrathalamic	3	Complete biodistribution
A09750	3: $1 \times 10e9$, 250 μl, intrathalamic	3	CNS biodistribution
30027	3: $1 \times 10e9$, 250 μl, intrathalamic	10	Complete biodistribution
A09158	3: $1 \times 10e9$, 250 μl, intrathalamic	10	CNS biodistribution
A10107	3: $1 \times 10e9$, 250 μl, intrathalamic	10	CNS biodistribution
A10129	3: $1 \times 10e9$, 250 μl, intrathalamic	10	CNS biodistribution
A09163	3: $1 \times 10e9$, 250 μl, intrathalamic	56	Select biodistribution, shedding, neutralizing antibodies
A08813	3: $1 \times 10e9$, 250 μl, intrathalamic	56	Select biodistribution, shedding, neutralizing antibodies
A09165	3: $1 \times 10e9$, 250 μl, intrathalamic	56	Shedding, neutralizing antibodies
A10103	3: $1 \times 10e9$, 250 μl, intrathalamic	56	Shedding, neutralizing antibodies

[a] For tissue inclusion with the biodistribution studies (complete, select, and CNS), see Table 4. Shedding studies included serum (viremia), saliva, urine, and stool samples.

TABLE 4 Biodistribution test regimens

Animals	Regimen	Testing schedule for biodistribution assays[a]
A08404, A08132, A08760, A09134, A09763, 30027	Complete	Adrenals, aorta, cecum, cerebrum, cerebellum, colon, CSF, duodenum, epididimy (in males), esophagus, eye, femur, gallbladder, gonads, heart, ileum, jejunum, kidney, liver, lung, mammary gland, mandibular LN, mediastinal LN, mesenteric LN, motor cortex, muscle, optic nerve, pancreas, pons/medulla, rib, salivary gland, sciatic nerve, skin, spinal cord, spleen, stomach, sternum, thymus, thyroid/parathyroid, tonsils, trachea, urinary bladder
A06682, A08813, A09163	Select	Cerebrum, cerebellum, colon, CSF, mandibular LN, mediastinal LN, mesenteric LN, motor cortex, pons/medulla, spinal cord
A09158, A09750, A10107, A10129	CNS	Cerebrum, cerebellum, CSF, motor cortex, pons/medulla, spinal cord

[a] CSF, cerebrospinal fluid; LN, lymph nodes.

sections of the needle track/site of the inoculum and five sections rostral and caudal, each, were prepared for histopathological analyses. To analyze viral spread, a series of sections spanning the entire brain, including the medulla oblongata, were prepared from both hemispheres. Neurohistopathological lesions extending from the inoculation site and needle track were carefully evaluated. The spread of virus from the inoculation site was assessed using criteria established with the WHO standard (47). These are cellular infiltration, cellular infiltration with minimal neuronal damage, cellular infiltration with extensive neuronal damage, and massive neuronal damage with or without cellular infiltration. The spinal cord was dissected *in toto* and preserved in cold, buffered neutral 10% formalin. Microscopic evaluation was focused on representative areas of the cervical (C7-C8) and lumbar (L4-L5) spinal cord. Five consecutive sections from each area were histopathologically analyzed.

Processing of simian tissues for biodistribution analyses. Fresh frozen tissue samples— 42 (for males) and 41 (for females)—removed from all macaques enrolled in the study (Table 3) were collected. The frozen samples chosen for further analyses (Table 4) were thawed at room temperature and placed on wet ice (4°C) thereafter. In a biosafety cabinet, the samples were placed in a sterile, disposable 5-ml tube. In a biosafety cabinet, 750 μl of sterile Roswell Park Memorial Institute (RPMI) medium containing antibiotics and an antimycotic (100 U penicillin/ml, 100 μg of streptomycin/ml, and 250 ng of amphotericin B/ml; Invitrogen) were added to the samples. The preprocessing weights of the nonosseous tissue samples (in a range from ~30 to ~300 mg), and the concentrations used in each assay were recorded for each sample. Using a BioGen Pro200 automated homogenizer equipped with an Multi-Gen 7-mm generator, the samples were homogenized at intervals of 15 s (level 1) to 15 s (level 5) to 15 s (level 5) to 15 s (level 5). The generator was rinsed with sterile PBS after each sample. The homogenized samples were placed on dry ice for snap-freezing following the homogenization procedure, thawed at room temperature, and centrifuged for 10 min at 8,000 rpm at 4°C to pellet remaining large debris. The supernatant was collected, divided into aliquots, and placed in sterile, disposable Eppendorf tubes. The pellet was discarded. The final, processed samples or aliquots thereof were either used immediately or refrozen on dry ice and transferred to −80°C for later analysis.

TCID$_{50}$ assay, plaque assay, and quantitative reverse transcription-PCR (qRT-PCR) analysis of tissue homogenates, sera and excreta. All TCID$_{50}$ assays of samples were performed immediately after sample processing and without intervening freezing steps. The samples were diluted 1:10, 1:20, 1:40, 1:80, 1:160, and 1:320 for TCID$_{50}$ assays according to the WHO standard (46, 47). For plaque assays, frozen aliquots of the samples were thawed for serial dilution in DMEM supplemented with 2% fetal bovine serum and antibiotic-antimycotic at 1:10, 1:100, and 1:1000. A total volume of 300 μl of DMEM containing the appropriate amount of diluted sample was added to confluent HeLa R19 cell monolayers grown overnight in sterile six-well plates. The covered plates were placed on a rocking device for 30 min at room temperature to facilitate virus binding. In a biosafety cabinet, 2 ml of overlay, consisting of 50:50 sterile, autoclaved tragacanth gum (3%; Sigma) at room temperature and 2× MEM (Invitrogen) at 37°C, was added to each well. The cells were incubated for

48 h at 37°C and fixed or stained thereafter by adding vital stain (1% crystal violet, 80% distilled H$_2$O, 20% methanol, 0.1% glutaraldehyde) to each well. The fixed/stained plates were placed on a rocking device for 30 min and rinsed thereafter.

The presence of viral genetic material in tissue samples/secreta was analyzed by qRT-PCR using methods described earlier (44). Briefly, total RNA was isolated from 200-μl samples using TRIzol reagent (Invitrogen) according to the manufacturer's instructions. To control for the presence of RNases in the samples, 100 ng of *in vitro* transcribed *Renilla* luciferase (*Rluc*) RNA was added to each sample prior to the isolation procedure. The generation of the *Rluc* reporter construct, *in vitro* transcription, and purification of the RNA are described elsewhere (11). A total of 25 ng of total RNA was used for each reaction performed with a TaqMan One-Step RT-PCR master mix reagent kit (Applied Biosystems; ABI) on an ABI 7900HT thermal cycler. Proprietary, custom-designed *Rluc* primers and FAM-labeled probe (ABI) were used to detect *Rluc*-positive control RNA. PVS2F forward primer (5′-AACCCAAT GTGTATCTAGTCGTAATGA-3′), PVS2R reverse primer (5′-TGAAAC ACGGACACCCAAAG-3′), and PVS2P probe (5′-[VIC]-CAATTGCGG GATGGGACCAACT-[TAMRA]-3′), all from ABI, were used for PVS-RIPO RNA detection. A standard curve with serial 10-fold dilutions of *in vitro*-transcribed PVS-RIPO RNA was included in every plate as a positive control. All measurements were taken in triplicate. The $\Delta\Delta C_T$ method was used to compare samples (24). The sensitivity of the assay was validated by including standard curves with defined amounts of viral genomic RNA. We regarded consistent cycle threshold (C_T) values (similar range in a triplicate reading) of <30 as significantly positive for viral RNA. This C_T value corresponds to ~625 templates/viral genomes.

Processing of excreta samples for biodistribution/shedding studies. All samples were collected from animals in the study as shown in Table 1. Each sample was thawed and processed individually as described below. The work area and all tools used were decontaminated with standard methods in between samples to avoid cross-contamination. Stool samples were subjected to homogenization and serial filtration to remove contaminating microbes. After thawing, 250 mg of each stool was placed in two sterile disposable 2-ml microcentrifuge tubes. Then, 1 ml of DMEM was added to each tube, and the samples were vigorously vortexed to produce a homogenate. The samples were centrifuged for 2 min at 10,000 rpm, and the resulting supernatant was pipetted into a sterile disposable 5-ml syringe (Becton Dickinson) and serially processed through sterile disposable 80-, 45-, and 20-μm filters (Pall Corp.). Saliva samples were expanded by addition of 500 μl of sterile PBS prior to further analyses. All saliva samples were sterile filtered by drawing the expanded sample into a sterile, disposable 3-ml syringe (Becton Dickinson) and expelling the sample through a sterile disposable 20-μm-pore-size filter (Pall Corp.). Urine samples were sterile filtered (using the same procedure used for saliva samples) only when bacterial contamination was evident in TCID$_{50}$ and plaque assays. The assays were repeated with the filtered sample. All serum samples were used unprocessed. All filtrates were used immediately for TCID$_{50}$ or stored at 20°C until further analysis by plaque assay or qRT-PCR.

Plaque neutralization assays. Neutralizing antibody titers in *M. fascicularis* were determined by plaque neutralization assay of serum samples
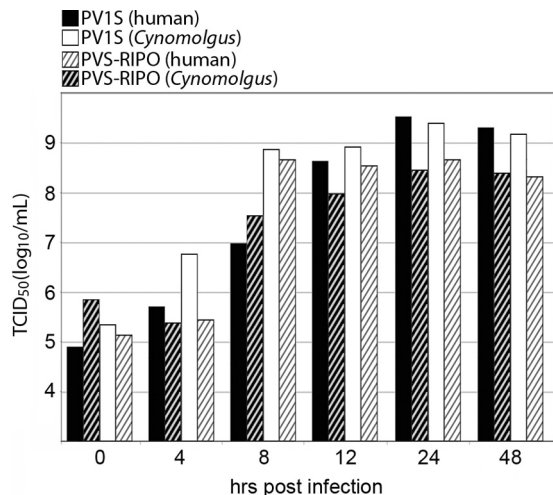
FIG 1 One-step growth curves in macaque and human primary explant renal cultures. PV1-S (solid bars) and PVS-RIPO (hatched bars) were propagated in *M. fascicularis* (black bars) or human (white bars) primary renal epithelial cells.

obtained as indicated in Table 1. The procedure used is described elsewhere (4).

RESULTS

***M. fascicularis* is an appropriate primate species for neurovirulence tests of PVS-RIPO.** To properly evaluate PVS-RIPO toxicity, biodistribution, shedding, and neutralizing antibody responses, experiments in nonhuman primates are mandated. In the past, a variety of Old World primate species have been used to test PV neurovirulence, but *M. fascicularis* emerged as the standard nonhuman primate species recommended by the WHO for tests of live-attenuated PV vaccines (47). We therefore considered *M. fascicularis* for toxicology evaluations of PVS-RIPO.

Since HRV2 does not naturally infect *M. fascicularis*, the presence of the heterologous HRV2 IRES may cause a host-specific virulence phenotype of PVS-RIPO in *M. fascicularis* cells. Efficient growth of multiple HRVs in primary explant *M. fascicularis* kidney cells does not support such a scenario (1), but we confirmed the absence of host effects on HRV2 IRES function in simians. To this end, we conducted susceptibility assays in primate explant kidney cells derived from human and *M. fascicularis* donors. The cells were tested at their second *ex vivo* passage by standard one-step growth curve assays (Fig. 1). We compared PVS-RIPO to its parent, PV1-S in this assay (Fig. 1). Our tests revealed that (i) both PV1-S and PVS-RIPO reach maximum progeny in human and macaque kidney cells by 24 h postinfection (p.i.), (ii) there was no propagation with either virus in *M. fascicularis* and human cultures beyond 24 h p.i., and (iii) cytopathic effects (CPE) were discernible in all infected cultures and progressed to overt cell lysis >50% by 48 h p.i. (data not shown). At 48 h p.i., the extent of CPE in PVS-RIPO and PV1-S-infected cultures was equivalent. Our tests also revealed that (iv) the overall growth efficiency at 12 h p.i. of PV1-S was ca. 2- to 3-fold higher than PVS-RIPO in both human and *M. fascicularis* kidney cells, (v) the propagation of both PV1-S and PVS-RIPO in macaque kidney cells was delayed at 8 h p.i. compared to human kidney cells (6.98 TICD$_{50}$/ml versus 8.81 TCID$_{50}$/ml for PV1-S and 7.54 versus 8.62 TCID$_{50}$/ml for PVS-RIPO), and (vi) the growth ratios in human versus *M. fascicularis*

primary kidney cells for PV1-S and PVS-RIPO were similar (Fig. 1). We conclude from our studies that the HRV2 IRES in PVS-RIPO does not exert species-specific effects on propagation and cytopathogenic potential in primary *M. fascicularis* kidney cells. We therefore proceeded with neurovirulence studies of PVS-RIPO in *M. fascicularis*.

Dose range-finding and definitive, IND-directed toxicology, biodistribution, and shedding studies of PVS-RIPO in *M. fascicularis*. To determine the safety, biodistribution and shedding of PVS-RIPO when introduced to *M. fascicularis* by the intrathalamic route, two separate studies were conducted with virus manufactured at the Biopharmaceutical Development Program, SAIC-Frederick, Inc. (see Materials and Methods). The first was a dose-range finding (DRF), toxicology, biodistribution, and shedding study involving nine animals assigned to four study groups (referred to as "DRF study" from here on; Table 2). Animals were inoculated with 10e7, 10e9, or 5 × 10e9 TCID$_{50}$ of PVS-RIPO or vehicle control by the intrathalamic route and sacrificed on study days 3 or 21 as shown (Table 2). The second was a definitive, IND-directed toxicology, biodistribution, shedding, and neutralizing antibody response study involving 30 animals assigned to three study groups (termed "IND-directed study" from here on; Table 3). Macaques received intrathalamic inoculations of 5 × 10e7 TCID$_{50}$ or 10e9 TCID$_{50}$ of PVS-RIPO or vehicle control by the intrathalamic route and were euthanized on study days 3, 10, or 56 (Table 3).

Clinical and pathological observations. The range of clinical and pathological tests conducted in conjunction with both studies is indicated in Materials and Methods. The results of these tests were consistent in both studies. Therefore, rather than listing the clinical or pathological study results for individual animals, the salient findings are summarized below. All animals enrolled in the DRF study (Table 2) survived PVS-RIPO intrathalamic challenge. Febrility and weight loss were not associated with PVS-RIPO inoculation in the animals. Few hematologic parameters and no clinical chemistry parameters consistent with viral infection were observed. The results of the DRF study suggest that PVS-RIPO remains contained within the brain after intrathalamic challenge, and no morbidity or mortality was associated with PVS-RIPO challenge in *M. fascicularis*. In the IND-directed study, all animals enrolled (Table 3) survived PVS-RIPO intrathalamic challenge. As observed before, febrility and weight loss did not occur in any of the animals and thrombocytosis was the only hematologic parameter associated with PVS-RIPO injection. No changes were noted in clinical chemistries consistent with viral infection. No ophthalmic changes were observed in any of the animals throughout the study. Physical exams revealed a decreased range of motion in the thoracic limbs in 20 of the 30 animals. However, this finding was also observed in the vehicle control-treated animals and is not likely due to treatment with PVS-RIPO. The outcome of the IND-directed study suggests that, similar to the DRF study, PVS-RIPO remains contained within the brain after intrathalamic challenge, and no mortality was associated with PVS-RIPO challenge in *M. fascicularis*.

Neurohistological analyses of the area of the virus inoculation site yielded consistent results for animals enrolled in both studies. The observed histological reactions were mainly ascribed to the inoculation procedure. Histopathological signs of active viral replication or viral central nervous system (CNS) lesions were absent in all animals in both studies. Therefore, we provide summary

descriptions of the salient histological findings below. The needle track and injection sites were identified in 8 of 9 and 5 of 9 of the animals in the DRF study, respectively (lesions could not be identified in the vehicle-treated monkey necropsied on study day 21). Needle track lesions were typically characterized by local hemorrhage, accumulation of phagocytic macrophages, astrogliosis, microgliosis, axon degeneration, and myelin sheath edema and, occasionally, local perivascular lymphocytic cuffing. The injection sites were generally located within or slightly forward of the anterior thalamus. For both the needle track lesions and the injection sites, there were only mild changes associated with the aging of the lesions, including the breakdown of hemoglobin into hemosiderin and the removal of necrotic cell debris by phagocytes. There was no evidence of expansion of neuronal necrosis that might signify virus spread. Only occasionally, lesions not confined to the immediate area surrounding the injection site or needle track occurred. These included minimal lymphocytic meningitis and rare, small foci of cerebral cortical microgliosis just below the meningeal space. There also were occasional small lymphocytic perivascular cuffs within the meninges surrounding the spinal cord, most often in sections from the cervical level. The lesions along the needle track and at the injection site were typical for an intracerebral injection. The only histopathologic findings that suggested a virus-induced CPE and/or antigen presentation were focal microgliosis and lymphocytic perivascular cuffs. These lesions were limited either to the immediate vicinity of the injection site or to rare, scattered foci within the meninges of the brain/spinal cord or the adjacent superficial cerebral cortex. There was no histopathologic evidence of lesions associated with direct virus spread away from the injection site in any of the sections examined and no difference in lesion severity based upon the size of the inoculum.

The needle track and injection sites were identified in all animals enrolled in the IND-directed study. Findings in PVS-RIPO-injected animals necropsied on study day 3 were characterized by local neuronal damage (which included axon degeneration and neuronal necrosis), accumulation of phagocytic macrophages, astrogliosis and microgliosis, and minimal to marked local hemorrhage. At the periphery of these regions of necrosis, there were a few small foci (fewer than 30 cells) of microgliosis associated with a small amount of necrotic cell debris and occasional blood vessels that were surrounded by small cuffs of lymphocytes and rare plasma cells. There was no evidence of expansion of neuronal necrosis beyond the immediate injection site that might signify virus spread. Only occasionally were lesions not confined to the immediate area surrounding the injection site or needle track, including minimal to mild lymphocytic meningitis and rare, small lymphocytic perivascular cuffs just below the meningeal space. There were also occasional small lymphocytic perivascular cuffs within the meninges surrounding the spinal cord. These more distant findings are likely a result of antigen leakage into the meningeal/ventricular spaces at the time of the injection and are not considered to represent true virus spread. There was no significant variation in the incidence or severity of the findings between the two PVS-RIPO-treated groups (Table 3). In the two vehicle control-treated animals necropsied at this time point the histopathological findings were similar, although without those attributed to antigenic stimulation (lymphocytic perivascular cuffing and lymphocytic meningitis). For PVS-RIPO-injected animals necropsied on study day 10, there were only mild changes associated with the aging of the lesions. Otherwise, the findings were

similar to those in animals necropsied on study day 3, although without evidence of lymphocytic meningitis, but with a small focus of microgliosis away from the injection site in one animal. In PVS-RIPO-injected animals necropsied on study day 56, aging of the lesions continued, with more prominent ceroid and little to no hemorrhage. Lesions in these animals were generally smaller than those at earlier time points. Lesions away from the injection site included minimal to mild lymphocytic cuffing and microgliosis in the brain, but no findings in the spinal cord. The two vehicle-treated animals had a similar diminution in injection site lesion size and severity as their PVS-RIPO-injected counterparts.

Altogether, the IND-directed and DRF studies yielded similar histopathological findings. Traumatic passage of the needle and injection of the inoculum accounts for the described hemorrhage, edema, and axon degeneration and the resulting cellular reaction that includes the local accumulation of phagocytic macrophages and astrogliosis. There was no histopathologic evidence of lesions associated with direct virus spread away from the injection site and no difference in lesion severity based upon the size of the inoculum.

PVS-RIPO biodistribution. Classic wt PV biodistribution studies after oral administration in chimpanzees suggest restrictive replication in select sites, including the primary sites of PV replication in the gastrointestinal tract and lymphatic structures associated with it and the secondary site in the CNS (2, 37). Since PVS-RIPO and PV1-S capsid structures are identical, and both depend on Necl-5 for host cell entry, it is reasonable to expect that both viruses share similar tissue tropism. However, it cannot be categorically ruled out that the heterologous HRV2 IRES in PVS-RIPO alters tissue type specificity. Also, a potential for extraneural dissemination of PVS-RIPO, which could be a prelude for shedding, is a safety concern for clinical administration by intracerebral inoculation. For these reasons, the biodistribution of PVS-RIPO after intrathalamic inoculation in *M. fascicularis* was studied. Biodistribution studies were included in both the DRF and the IND series, with concordant results in all animals enrolled in all experimental groups in both studies. For brevity, only the results of the IND-directed studies are discussed. To limit the burden of these extensive studies, not all animals (or not all samples from all animals) were tested for PVS-RIPO biodistribution. The inclusion of study subjects and the biodistribution/shedding test schedules used for each animal are indicated in Table 2 (for the DRF study) and Table 3 (for the IND-directed study). Since the study results were consistent in both studies, we provide summary descriptions of the salient findings rather than listing study results for individual animals.

First, we conducted "complete" biodistribution studies in four macaques euthanized at 3 days and two macaques euthanized at 10 days after inoculation, respectively (Table 3). Only animals in the vehicle control group and the high-dose group were tested (Table 3). Complete biodistribution included analyses of 42 (male) or 41 (female) tissue samples that were collected from the euthanized animals (Table 4). All tissue samples were homogenized and subjected to parallel $TCID_{50}$ assay, plaque assay, and qRT-PCR analysis (see Materials and Methods). There was no indication for infectious material in $TCID_{50}$ or plaque assays from any extraneural tissue sample recovered from any animal at any study interval. Accordingly, qRT-PCR of RNA recovered from tissue homogenates did not reveal the presence of viral genetic material in any extraneural tissue. This indicates that extraneural

dissemination with replication in extraneural tissues does not occur after intracerebral inoculation of 10e9 $TCID_{50}$ of PVS-RIPO in the IND-directed study or $5 \times$ 10e9 $TCID_{50}$ of PVS-RIPO in the DRF study.

In one animal in the IND-directed study of the high-dose group euthanized at study day 3 (A09763: Table 3), PVS-RIPO was isolated from spinal cord and pons/medulla tissue samples. The titers recovered in $TCID_{50}$ and plaque assays were similar and indicated concentrations of PVS-RIPO of 1.01 PFU/mg (pons/medulla) and 0.83 PFU/mg (spinal cord), respectively. Due to the very low viral load and the absence of corresponding gross pathological, histopathological, or neurological signs of acute virus-induced lesions, we hypothesize that this material is the inoculum. The sensitivity of our biodistribution assays can be gauged from these positive samples. The results of $TCID_{50}$/plaque assays for both samples were consistent, as expected from these infectivity tests. Our results imply a detection threshold of ~833 PFU/g, which is well below the titers typically found in known poliovirus reservoir sites in primates, e.g., 16,000 PFU/g in Peyer's patches of an orally infected chimpanzee (2). The sensitivity threshold of the qRT-PCR tests was at ~625 templates (see Materials and Methods). Infectivity assays suggest that none of the biodistribution samples, including the two positive samples from animal A09763, contained viral RNA in quantities at or above the detection threshold for qRT-PCR.

Since extraneural dissemination of PVS-RIPO was not detected in any animal analyzed and virus was recovered from CNS tissues in one case, we performed "CNS biodistribution" analyses of all remaining animals in the high-dose group euthanized at study days 3 and 10 (Table 3). These included $TCID_{50}$ assays, plaque assay, and qRT-PCR analyses of homogenates of six CNS tissues (Table 4). None of these tests revealed the presence of PVS-RIPO in any sample. To test for the possible persistence of PVS-RIPO after intracerebral inoculation, we tested the presence of PVS-RIPO in known sites of PV susceptibility ("select biodistribution" [Table 4]) in three animals euthanized at 56 study days (Table 3). The tests included animals in the vehicle control and high-dose groups (Table 3). $TCID_{50}$ assays, plaque assays, and qRT-PCR tests of the tissue homogenates analyzed did not reveal the presence of PVS-RIPO at any site.

PVS-RIPO viremia and shedding. Replication of PV in the gastrointestinal tracts of susceptible primates (25) or humans (20) leads to shedding of live virus with stool. It has been observed in several primate studies that intracerebral inoculation of wt PVs does not produce shedding (3, 7). This may be explained by the absence of an obvious route that could disseminate virus from an inoculation site in the CNS to the gastrointestinal tract. Active viral replication in gastrointestinal epithelium likely is a prerequisite for PV shedding with stool.

Both primate experiments reported here included thorough analysis of PVS-RIPO dissemination from the intrathalamic inoculation site by viremia (virus in serum) and possible shedding of the virus with saliva, urine or, most importantly, stool. The DRF and IND-directed toxicology studies yielded identical results for all parameters tested in all animals enrolled in the study. For brevity, only the results of the IND-directed toxicology study are discussed. To favor the detection of shed virus and to enable longitudinal shedding analyses, animals in the high-dose group euthanized at study day 56 were included (A09163, A08813, A09165, and A10103; Table 3). A schedule of the collection inter-

vals and the types of samples obtained is shown in Table 1. All samples included in the study were analyzed by parallel $TCID_{50}$ assay, plaque assay, and qRT-PCR for the detection of viral genetic material.

Serum is of central importance for the biodistribution and shedding studies reported here because (i) viremia occurs with natural PV infection of humans, (ii) viremia occurs with experimental oral PV infection of nonhuman primates (2, 37), and (iii) hematogenous spread is the most plausible route of dissemination after intracerebral inoculation. D. Bodian (2) reported a virus load of 40,000 $TCID_{50}$ per g of serum at 4 days after oral administration in a chimpanzee. In similar assays (at 3 days after intrathalamic administration), we tested 20 μl (for the lowest dilution for $TCID_{50}$ assays) or 30 μl (for the lowest dilution for plaque assays) of serum, which is equivalent to roughly 20 or 30 mg, respectively. Assuming that our tests would detect a single infectious unit in serum, the theoretical threshold of detection of our tissue culture-based assays is 800- to 1,200-fold above the levels of viremia reported previously by Bodian (2). No infectious material was detected by either assay at any study day in any of the animals tested (Table 3).

For saliva, due to the small sample amounts ($<$100 μl in all cases), the samples were expanded by addition of 500 μl of sterile PBS. Due to the likely presence of bacterial contaminants, all samples were sterile filtered (Materials and Methods). $TCID_{50}$ assays and plaque assays included analysis of 1:10 dilutions of the starting material. Assuming that a single infectious unit would have been detected in either assay, the sensitivity of our tests is estimated at ca. 18 to 25 infectious particles per average sample of ~75 μl. $TCID_{50}$ assays and plaque assays revealed the absence of infectious material in all samples, and qRT-PCR failed to detect viral genetic material in saliva samples at any study day in any of the animals tested (Table 3).

PV is not known to be excreted with urine from infected individuals. Urine samples included in the study were either unfiltered or were filtered if bacterial contamination was evident in the tissue culture-based assays for repeat studies. $TCID_{50}$ assays, plaque assays, and qRT-PCR did not reveal the presence of infectious virus or viral genetic material in urine from any animal at any study interval.

Since excretion with stool is the natural dissemination route of PVs from infected persons, particular emphasis was placed on this study parameter. PVS-RIPO shedding studies included the analysis of stool samples from animals in the high-dose group (A09163, A08813, A09165, and A10103; Table 3) at study days 3, 10, 12, 14, 15, 18, 21, 25, 28, 35, 43, 49, and 56 (Table 1). Analysis of stool samples by $TCID_{50}$ assay, plaque assay, and qRT-PCR at all study intervals did not indicate the presence of PVS-RIPO in stool samples from any animal enrolled in the study. These results are concordant with the lack of viremia or extraneural dissemination to the gastrointestinal tract after intracerebral PVS-RIPO inoculation in *M. fascicularis*.

Poliovirus neutralizing antibody titers in *M. fascicularis*. To determine whether macaques receiving intrathalamic inoculations of PVS-RIPO mount an anti-poliovirus immune response, plaque neutralization assays were performed according to established protocols (4). Only animals in the IND-directed study were tested (Table 5). Study subjects included macaques in the high-dose group 3 euthanized at study day 56 and corresponding animals from the vehicle control group 1 (Table 3). Test samples

TABLE 5 Results of plaque neutralization assays of macaque sera

Animal (group)	Day	Antibody titer
A09163 (3)	0	<4
	3	<4
	10	133
	28	256
	56	426
A08813 (3)	0	<4
	3	56
	10	640
	28	1,024
	56	914
A09165 (3)	0	8
	3	8
	10	1,280
	28	2,560
	56	6,400
A10103 (3)	0	<4
	3	<4
	10	64
	28	192
	56	916
A06682 (1)	0	8
	3	8
	10	8
	28	8
	56	8
A06953 (1)	0	<4
	3	<4
	10	<4
	28	<4
	56	<4

included sera obtained at study days 0, 3, 10, 28, and 56 (Table 1). All animals tested showed signs of a neutralizing, anti-poliovirus antibody response by day 10. Neutralizing antibody titers in all animals increased significantly by study day 56 (Table 5). None of the animals in the vehicle control group showed signs of an immunologic response against poliovirus at any time (Table 5).

DISCUSSION

PVS-RIPO, which is fully replication competent in susceptible tissue culture cells (e.g., Vero [*C. aethiops* kidney] cells) or the intended GBM target (17), exhibits extraordinarily low neurovirulent potential after intrathalamic inoculation in *M. fascicularis*. Inoculation of up to $5 \times 10e9$ TCID$_{50}$ of PVS-RIPO did not produce neurohistopathological lesions, clinical neurological symptoms, or other signs of active viral replication in the primate CNS. There were no hematologic or clinical chemical parameters consistent with active viral replication. There was no evidence for viremia, extraneural spread, extraneural replication, or shedding of PVS-RIPO with saliva, urine, or stool. Our findings suggest that the intrathalamic virus inoculum remains contained within the CNS of injected animals. The primate neurovirulence assays described here are concordant with the results of previous empirical studies in neuron-like tissue culture models (5, 16, 17, 27, 48), in mice transgenic for human *Necl-5* (15, 16) and in *M. fascicularis*

challenged with intraspinal inoculation of PV1-RIPO (16). Our investigations confirm a dominant role for the IRES and, hence, ribosome recruitment to viral RNAs in PV pathogenesis.

Mechanistic studies of neuronal incompetence of the foreign HRV2 IRES in PVS-RIPO revealed deficits in ribosome recruitment. Since PVS-RIPO translation is unencumbered in transformed cells, such deficits are likely due to tissue type-specific host conditions in the normal CNS. For the type 1 picornaviral IRES, ribosome recruitment relies on direct interactions with eIF4G (8). Thus, the PV-S/HRV2 IRES may exhibit deficits attracting eIF4G in the normal CNS. Indeed, genetic signatures responsible for neuroattenuation mediated by the PV-S IRES (8, 33) or the HRV2 IRES (5, 16) map to structures that participate in eIF4G contacts.

Multiple, not mutually exclusive events may dictate IRES function in the host CNS by controlling eIF4G-IRES interactions. Most directly, PVS-RIPO translation may be determined by the functional state of eIF4G itself. In GBM cells, supporting rampant PVS-RIPO translation (implying efficient IRES function [17]), constitutively active signal transduction pathways converge on eIF4G and its binding partners. We showed that activation of the protein kinase C-α (PKC-α)-Erk1/2 mitogen-activated protein kinase (MAPK) signaling axis with phorbol esters leads to phosphorylation of eIF4G(Ser1186) (by PKC-α) and eIF4G(Ser1232) [by a currently unknown kinase(s)] (9). Phosphorylation of eIF4G(Ser1186) and activation of Erk1/2 MAPKs induces MAPK signal integrating kinase 1 (Mnk1) binding to eIF4G (38), which is required for phosphorylation of eIF4E by Mnk1 (35). We showed that signaling through Erk1/2 to MAPK signal integrating kinase 1 (Mnk1) determines PVS-RIPO translation and cytotoxicity in GBM (14). Accordingly, providing constitutively active Mnk1 in neuron-like cells stimulates viral, HRV2 IRES-mediated translation and reverses the CNS deficit of PVS-RIPO (14). MAPK signal transduction to protein synthesis machinery may favor viral cap-independent translation by stimulating the formation of translation-competent RNPs via recruitment of eIF4G to the IRES.

Indirectly, IRES-eIF4G interactions may be influenced through host RNA-binding, IRES *trans*-acting factors (ITAFs). The double-stranded RNA-binding protein 76 (DRBP76) associates with the HRV2 IRES specifically in neuronal cells (27) and intercepts IRES-mediated translation initiation (28). A physiologic function of DRBP76 in translation repression at invading viral genomes, possibly as part of an antiviral defense mechanism, has been proposed (18). Since ITAFs may also favor eIF4G-IRES binding (22), positive contributors to an IRES ribonucleoprotein (RNP) complex conducive to eIF4G recruitment may be lacking in the CNS or may be displaced by DRBP76. We showed that DRBP76 exhibits distinct properties in GBM compared to brain. Most importantly, it is almost exclusively nuclear in GBM versus predominantly cytoplasmic in brain (30). Thus, lacking ribosome recruitment at the HRV2 IRES in the normal CNS may reflect the array of cytoplasmic RNA-binding proteins encountered by PVS-RIPO.

For comparison of their neurovirulent potential, we contemplated including the PVS-RIPO precursor, PV1-S, in our studies. Since the studies were designed to support regulatory evaluation of PVS-RIPO, this was not pursued. Although they cannot replace primate studies, mechanistic investigations of neuronal IRES competence offer insight into this issue. Compared to wt PV1, both PV1-S and PVS-RIPO share significant translation, replica-

tion, and cell-killing deficits in HEK-293 neuroblastoid cells (5). These are far more pronounced for PVS-RIPO compared to PV1-S (48), suggesting lower neuronal IRES competence due to inherently impaired eIF4G recruitment to the foreign HRV2 IRES. This assumption is supported by differences in the genetic basis for neuronal IRES deficits. In PV1-S, they rely on a single nucleotide substitution, G480A, in IRES SLD V (8, 33). In contrast, IRES incompetence of PVS-RIPO rests on a broad, discontinuous, and structurally complex base comprising SLDs V and VI in the HRV2 IRES (5, 16). Interestingly, eIF4G/eIF4A interactions with picornavirus type 1 IRES involve the same structures (8).

This contrast is also evident when considering the most significant safety shortcoming of PV-S, genetic instability. The G480A IRES mutation in PV1-S spontaneously and rapidly reverts to wt upon propagation in Vero cells (19). Such adaptation events do not occur with PVS-RIPO (10). This suggests that eIF4G recruitment deficits of PV1-S, due to a single IRES mutation acquired upon artificial selection *in vitro*, are shallow compared to those in PVS-RIPO, encrypted by a naturally evolved IRES element. Therefore, we stipulate that neuroattenuation of PVS-RIPO is at least at level with PV1-S, if not significantly lower. This is supported by neurovirulence tests of PV1-S and PV1-RIPO after intraspinal inoculation in *M. fascicularis* (16).

We document safety of PVS-RIPO in terms of low neuropathogenicity, inability to disseminate or replicate extraneurally, and lack of shedding. Our studies support the clinical use of PVS-RIPO as a direct oncolytic, indirect immunotherapeutic agent against GBM.

ACKNOWLEDGMENTS

REFERENCES

1. **Andeweg AC, Bestebroer TM, Huybreghs M, Kimman TG, de Jong JC.** 1999. Improved detection of rhinoviruses in clinical samples by using a newly developed nested reverse transcription-PCR assay. J. Clin. Microbiol. **37**:524–530.
2. **Bodian D.** 1955. Emerging concept of poliomyelitis infection. Science **122**:105–108.
3. **Bodian D, Howe HA.** 1945. Non-paralytic poliomyelitis in the chimpanzee. J. Exp. Med. **81**:255–274.
4. **Boone EJ, Albrecht P.** 1983. Conventional and enhanced plaque neutralization assay for polio antibody. J. Virol. Methods **6**:193–202.
5. **Campbell SA, Lin J, Dobrikova EY, Gromeier M.** 2005. Genetic determinants of cell type-specific poliovirus propagation in HEK 293 cells. J. Virol. **79**:6281–6290.
6. **Castriconi R, et al.** 2009. NK cells recognize and kill human glioblastoma cells with stem cell-like properties. J. Immunol. **182**:3530–3539.
7. **Clark PF, Schindler J.** 1932. Passage of poliomyelitis virus through the intestinal tract. J. Prev. Med. **6**:47–58.
8. **de Breyne S, Yu Y, Unbehaun A, Pestova TV, Hellen CU.** 2009. Direct functional interaction of initiation factor eIF4G with type 1 internal ribosomal entry sites. Proc. Natl. Acad. Sci. U. S. A. **106**:9197–9202.
9. **Dobrikov M, Dobrikova E, Shveygert M, Gromeier M.** 2011. Phosphorylation of eukaryotic translation initiation factor 4G1 (eIF4G1) by protein kinase C-α regulates eIF4G1 binding to Mnk1. Mol. Cell. Biol. **31**:2947–2959.
10. **Dobrikova EY, et al.** 2008. Recombinant oncolytic poliovirus eliminates glioma in vivo without genetic adaptation to a pathogenic phenotype. Mol. Ther. **16**:1865–1872.
11. **Dobrikova EY, Grisham RN, Kaiser C, Lin J, Gromeier M.** 2006. Competitive translation efficiency at the picornavirus type 1 internal ribosome entry site facilitated by viral cis and trans factors. J. Virol. **80**:3310–3321.
12. **Evans DM, et al.** 1985. Increased neurovirulence associated with a single nucleotide change in a noncoding region of the Sabin type 3 poliovaccine genome. Nature **314**:548–550.
13. **Florez de Sessions P, Dobrikova E, Gromeier M.** 2007. Genetic adaptation to untranslated region-mediated enterovirus growth deficits by mutations in the nonstructural proteins 3AB and 3CD. J. Virol. **81**:8396–8405.
14. **Goetz C, Everson RG, Zhang LC, Gromeier M.** 2010. MAPK signal-integrating kinase controls cap-independent translation and cell type-specific cytotoxicity of an oncolytic poliovirus. Mol. Ther. **18**:1937–1946.
15. **Gromeier M, Alexander L, Wimmer E.** 1996. Internal ribosomal entry site substitution eliminates neurovirulence in intergeneric poliovirus recombinants. Proc. Natl. Acad. Sci. U. S. A. **93**:2370–2375.
16. **Gromeier M, Bossert B, Arita M, Nomoto A, Wimmer E.** 1999. Dual stem-loops within the poliovirus internal ribosomal entry site control neurovirulence. J. Virol. **73**:958–964.
17. **Gromeier M, Lachmann S, Rosenfeld MR, Gutin PH, Wimmer E.** 2000. Intergeneric poliovirus recombinants for the treatment of malignant glioma. Proc. Natl. Acad. Sci. U. S. A. **97**:6803–6808.
18. **Harashima A, Guettouche T, Barber GN.** 2010. Phosphorylation of the NFAR proteins by the dsRNA-dependent protein kinase PKR constitutes a novel mechanism of translational regulation and cellular defense. Genes Dev. **24**:2640–2653.
19. **Horie H, et al.** 2001. Analysis of the accumulation of mutants in Sabin attenuated polio vaccine viruses passaged in Vero cells. Vaccine **19**:1456–1459.
20. **Howe HA, Bodian D.** 1940. Untreated human stools as a source of poliomyelitis virus. J. Infect. Dis. **66**:198–201.
21. **Jang SK, et al.** 1988. A segment of the 5′ nontranslated region of encephalomyocarditis virus RNA directs internal entry of ribosomes during in vitro translation. J. Virol. **62**:2636–2643.
22. **Kafasla P, Morgner N, Robinson CV, Jackson RJ.** 2010. Polypyrimidine tract-binding protein stimulates the poliovirus IRES by modulating eIF4G binding. EMBO J. **29**:3710–3722.
23. **Kawamura N, et al.** 1989. Determinants in the 5′ noncoding region of poliovirus Sabin 1 RNA that influence the attenuation phenotype. J. Virol. **63**:1302–1309.
24. **Lowe B, Avila HA, Bloom FR, Gleeson M, Kusser W.** 2003. Quantitation of gene expression in neural precursors by reverse-transcription polymerase chain reaction using self-quenched, fluorogenic primers. Anal. Biochem. **315**:95–105.
25. **Melnick JL.** 1946. The recovery of poliomyelitis virus from the stools of experimentally infected monkeys and chimpanzees. J. Immunol. **53**:277–290.
26. **Merrill MK, et al.** 2004. Poliovirus receptor CD155-targeted oncolysis of glioma. Neuro-Oncology **6**:208–217.
27. **Merrill MK, Dobrikova EY, Gromeier M.** 2006. Cell-type-specific repression of internal ribosome entry site activity by double-stranded RNA-binding protein 76. J. Virol. **80**:3147–3156.
28. **Merrill MK, Gromeier M.** 2006. The double-stranded RNA binding protein 76:NF45 heterodimer inhibits translation initiation at the rhinovirus type 2 internal ribosome entry site. J. Virol. **80**:6936–6942.
29. **Minor PD, Macadam AJ, Stone DM, Almond JW.** 1993. Genetic basis of attenuation of the Sabin oral poliovirus vaccines. Biologicals **21**:357–363.
30. **Neplioueva V, Dobrikova EY, Mukherjee N, Keene JD, Gromeier M.** 2010. Tissue type-specific expression of the dsRNA-binding protein 76 and genome-wide elucidation of its target mRNAs. PLoS One **5**:e11710.
31. **Nomoto A, Lee YF, Wimmer E.** 1976. The 5′ end of poliovirus mRNA is not capped with m7G(5′)ppp(5′)Np. Proc. Natl. Acad. Sci. U. S. A. **73**:375–380.
32. **Nomoto A, et al.** 1982. Complete nucleotide sequence of the attenuated

poliovirus Sabin 1 strain genome. Proc. Natl. Acad. Sci. U. S. A. **79**:5793–5797.

33. **Ochs K, et al.** 2003. Impaired binding of standard initiation factors mediates poliovirus translation attenuation. J. Virol. **77**:115–122.

34. **Pelletier J, Sonenberg N.** 1988. Internal initiation of translation of eukaryotic mRNA directed by a sequence derived from poliovirus RNA. Nature **334**:320–325.

35. **Pyronnet S, et al.** 1999. Human eukaryotic translation initiation factor 4G (eIF4G) recruits Mnk1 to phosphorylate eIF4E. EMBO J. **18**:270–279.

36. **Sabin AB.** 1960. Oral, live poliovirus vaccine for elimination of poliomyelitis. Arch. Intern. Med. **106**:5–9.

37. **Sabin AB.** 1956. Pathogenesis of poliomyelitis; reappraisal in the light of new data. Science **123**:1151–1157.

38. **Shveygert M, Kaiser C, Bradrick SS, Gromeier M.** 2010. Regulation of eukaryotic initiation factor 4E (eIF4E) phosphorylation by mitogen-activated protein kinase occurs through modulation of Mnk1-eIF4G interaction. Mol. Cell. Biol. **30**:5160–5167.

39. **Sloan KE, et al.** 2004. CD155/PVR plays a key role in cell motility during tumor cell invasion and migration. BMC Cancer **4**:73.

40. **Sloan KE, Stewart JK, Treloar AF, Matthews RT, Jay DG.** 2005. CD155/PVR enhances glioma cell dispersal by regulating adhesion signaling and focal adhesion dynamics. Cancer Res. **65**:10930–10937.

41. **Sutter RW, Cochi SL, Melnick JL.** 1999. Live attenuated poliovirus vaccines, p 364–408. *In* Plotkin SA, Orenstein WA (ed), Vaccines, 3rd ed. W. B. Saunders, Philadelphia, PA.

42. **Takai Y, Miyoshi J, Ikeda W, Ogita H.** 2008. Nectins and nectin-like molecules: roles in contact inhibition of cell movement and proliferation. Nat. Rev. Mol. Cell. Biol. **9**:603–615.

43. **Toyoda H, Yin J, Mueller S, Wimmer E, Cello J.** 2007. Oncolytic treatment and cure of neuroblastoma by a novel attenuated poliovirus in a novel poliovirus-susceptible animal model. Cancer Res. **67**:2857–2864.

44. **Walters RW, Bradrick SS, Gromeier M.** 2010. Poly(A)-binding protein modulates mRNA susceptibility to cap-dependent miRNA-mediated repression. RNA. **16**:239–250.

45. **Wimmer E, Hellen CU, Cao X.** 1993. Genetics of poliovirus. Annu. Rev. Genet. **27**:353–436.

46. **World Health Organization.** 2002. Recommendations for the production and control of poliomyelitis vaccine (oral). World Health Organ. Tech. Rep. Ser. **910**:1–104.

47. **World Health Organization.** 1990. Requirements for poliomyelitis vaccine (oral). World Health Organ. Tech. Rep. Ser. **800**:30–86.

48. **Yang X, et al.** 2009. Evaluation of IRES-mediated, cell-type-specific cytotoxicity of poliovirus using a colorimetric cell proliferation assay. J. Virol. Methods **155**:44–54.